Sensors & Transducers, Vol. 264, Issue 1, February 2024, pp. 26-33

www.sensorsportal.com

Sensors & Transducers

Published by IFSA Publishing, S. L., 2024
http://www.sensorsportal.com

A Novel Large Travel, High Precision MEMS Based Electro-thermal Linear Actuator for Adjusting CCD Camera Lens

Ehsan Atash ZABAN and Dr Mehmet KUSAF
Department of Electrical and Electronic Engineering,
Cyprus International University, 99258, Nicosia, Northern Cyprus, Mersin, 10, Turkey
Tel: 00989375437106
E-mail: 22009479@student.ciu.edu.tr, mkusaf@ciu.edu.tr

Received: 16 December 2024 /Accepted: 28 December 2024 /Published: 28 February 2024

Abstract: In this paper, a linear micro actuator (*LMA*) with a stroke of 2.1 μm is designed and presented. Substrate, springy slider, and stopper are main parts of the *LMA* proposed. A large travel range can be achieved, by repeating the generated strokes. All simulations are done with *ANSYS* finite element. The springy slider, particularly and interestingly, can be deformed bidirectional either up-ward or down-ward. In fact, the slider creates such a linear deformation in one direction by electro-thermal stimulation. Without a stabilizer there is no value in even making such linear deformation. To stabilize and to prepare the slider for a large travel range, the four stoppers includes the springy clutches and electrostatic comb drives are used. The comb drives works with the electrostatic actuation and generates the propulsion forces required of the springy clutches. The clutches touches the side wall of the substrate to hold and stable the slider´s stroke. Combining the stroke of the slider and the stoppers operation, results a large travel range interestingly. The *LMAs* with large travel range are so important for different kinds of applications in micrometer scales. This *LMA* can push and pull the loady objects connected to the slider´s head accurately and can be used in adjusting CCD camera lens.

Keywords: MEMS, CCD camera lens, The *LMA*, The slider, The stopper, Stroke, The Clutch, The electro-thermal actuators.

1. Introduction

The *LMAs* play an important role in micro-electro-mechanical-systems (*MEMS*). They can be the main components of the artificial arms and the muscles so that can strengthen the dynamic parameters of the robots because of their light-weight, micrometric scale and their own output force generated. These actuators have many applications in the industrials and the scientific equipment's; for example, the MRI resonance image scanners and the electron beam lithography systems. There are different kinds of actuators working on complex and sensitive micro systems such as the electro-thermal, the electrostatic, the piezoelectric, and the magnetic and so on [3, 4, 7]. All the micro actuators mentioned have their relative advantages and disadvantages, particularly. As an example, the magnetic *LMAs* can have a significant negative effect on the entire micro scale systems, so the non-magnetic ones can be proposed and substituted [15, 2]. The resolution, the stroke and the speed are the parameters to be taken into account during designing. The force generated by the electro-static micro-actuators is too small. Therefore, to increase the deformation, the voltage applied should be increased. The piezoelectric micro actuator are powerful and can displace heavy loads but due to the

problems of using the piezoelectric materials in the process of layering, casting in micrometric cases and achieving the displacement of more than one millimeter, the specialists of such systems are focused on the electro-thermal systems, instead. To create a linear motion actually in a certain direction, there are some methods. Firstly, the slider of micro-motor can be moved through transferring motions between a series of impacts. Second methods are the impact heads toothed engaged with the slider, which causes the slider to have a high output force [11, 10, 16, 7]. In the third method, the slider is held through the friction generated between the clutch of a stopper and either the contact surfaces or the substrate side walls [1, 14]. In this work, a novel *LMA* with a force generated up to 2 mN and a large travel range, with high precision, is going to be proposed. One of the interesting goals in the designing such micro actuators is to achieve high precision stroke. Another point in designing of these actuators is to achieve the large travel ranges so that *LMAs* can be applied in some important applications like adjusting CCD Camera Lenses [21, 12]. In the Section 2.1 of the paper, the mechanism of the linear actuator proposed is explained. Afterward, the slider is analyzed and equations due to designing are presented (Section 2.2); paper explains the stopper (Section 2.3). In the final, the conclusion is presented.

2. Design

2.1. Mechanism

The micro-actuator proposed, as it can be shown in Fig. 1, has three main parts; the substrate, the slider and the stoppers. The substrate acts as a chassis and the springy slider consists of the beams (hot arms), the electrical electrodes, and the constrainer. The stopper assembles on the four corners of the springy slider´s upper surface. In other words, there are the four stoppers placed on the surface of the slider. The stoppers include the springy clutch, and electrostatic comb drives. The clutches are used to prevent the slider from moving or randomly shaking and the electrostatic comb drives are used to generate the force required for connecting the clutches to the substrate side walls. As it said, in the normal state, all the clutches' heads are connected to the substrate side wall to prevent the slider from shaking and vibrating. Thickness of the slider, the comb drives and the clutch are 5 μm, 3.5 μm and 3.5 μm, respectively. Two sets of the electrodes are located in up and down sections of the slider to stimulate the springy electro-thermal actuator. When the slider is in the rest mode, all of the clutches are connected to the substrate side wall. For an up-ward or down-ward deformation, an actuation voltage is required to be applied to the electro-thermal slider electrode which causes an electrical current flowing through the hot arms. To lock the four corners of the slider from any randomly shaking or instability, the four comb drives remain activated.

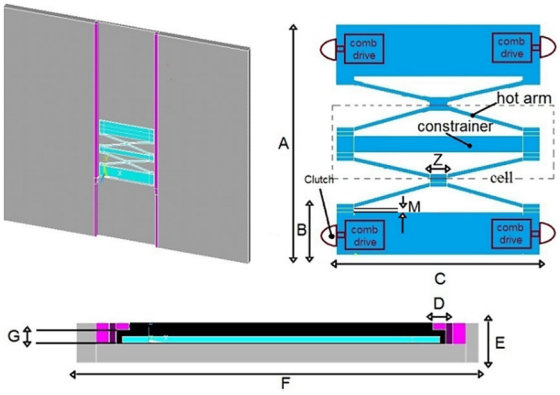

Fig. 1. Structure of the linear micro actuator.

In the normal mode, the entire stoppers are activated and positive voltages are connected to all of the electrostatic comb-drives' electrodes 1, 2, 3, 4 and the electro-thermal slider electrodes' voltage would be zero, please see Fig. 2 (a). To start an up-ward deformation, the DC positive voltage is connected to the electro-thermal slider electrode which causes up-warding expansion; takes into account the comb drives 3, 4 should be cut off, see Fig. 2 (b).

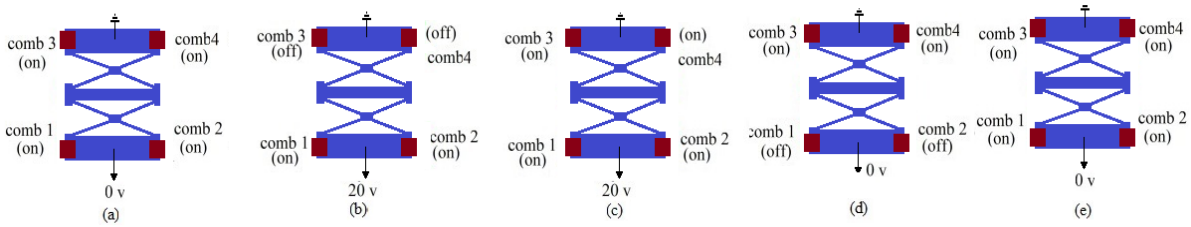

Fig. 2. Motion cycles of the slider.

To save the deformation generated after expanding the slider, the voltages of the comb drives 1, 2, 3, 4 remain ON; ON, actually, here means the positive DC voltage is connected, see Fig. 2(c). To stabilize the whole system and store the built-in up-ward deformation, the positive DC voltage is applied to all comb drives. The electrode´s voltage of the slider and the combs 1, 2 remain cut off so that the slider can be

ready to contract through the temperature returning, see Fig. 2 (d). This contraction causes the down part of the slider have an up-ward movement. To achieve a backward movement, the orders of the applied signals can be reversed. Fig. 3 shows the different voltages applied to the *LMA*; T_{sw} is the rest time of the slider. In this period of time, the slider stays off., $T_{gw1,2}$ is ON till the slider goes cold.T_{go1} is rest time of the stoppers 1, 2 and T_{go2} is rest time of the stoppers 3, 4 to next cycle. The combs 1, 2, 3, 4 are ON and the slider voltage remains 0 volt. By repeating the process above, the slider can achieve a long linear up-ward movement. For a down-ward movement, all previous steps can be done reversely. To reach a high precision and large travel range, all parameters carefully and separately should take into consideration [19, 9]. To fabricate a prototype of such complex linear actuator, all dimensions, geometries, material properties of the linear actuator narrowly must be calculated and analyzed.

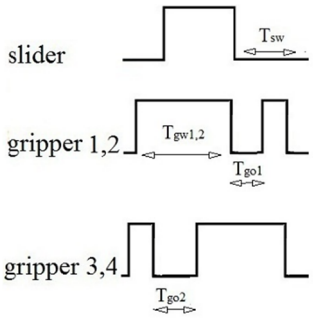

Fig. 3. The signals applied.

2.2. Slider Thermal Equations

Before embarking into designing and simulation of the slider, we take into account analysis of Electro-thermal equations related to the slider. Since length of the hot arms inclined is much larger than height and width, a model simplified shown in Fig. 4, and related deformation calculations can be considered, see Fig. 5. L, h and w are length, height and the width of the model mentioned. By neglecting the heat loses caused by radiation and convection than the ambient, heat conduction would be as following [17, 7, 8]:

$$Q = -K\,A\frac{\partial T}{\partial x} \tag{1}$$

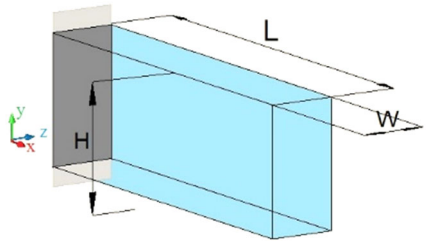

Fig. 4. The Model simplified.

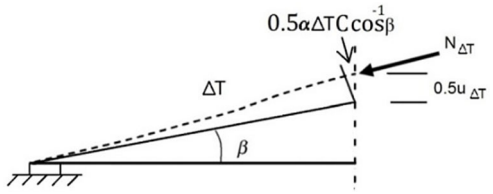

Fig. 5. Mathematical model of the beams.

In the equation above, K, A and x presents the thermal conductivity of polysilicon, temperature, cross-section and variable length of the mode, respectively. By passing the heat through the structure, we have:

$$Q_{input} = -K\,wh\left(\frac{\partial T}{\partial x}\right)_x \tag{2}$$

Output heat conduction is (3):

$$Q_{output} = -K\,wh\left(\frac{\partial T}{\partial x}\right)_{x+dx} \tag{3}$$

The structure can be treated as an electrical circuit by applying an actuation voltage between two electrodes:

$$Q_J = \left(\frac{v}{\rho L}\right)^2(\rho_0[1+\zeta(T-T_0)])whdx, \tag{4}$$

where v, ρ_0, T_0 and ζ are the actuation voltage, the special resistance of the model at temperature of T_0, the normal temperature of substrate electrodes that consider $293K_0$ and temperature coefficient, respectively.

$$Q_{input} + Q_J = Q_{output} \tag{5}$$

By substituting Equations (2) and (4) into Equation (5), and considering dx→0, the following equation achieves:

$$K_p\left(\frac{\partial_2 T}{\partial x^2}\right) = -j^2\rho \tag{6}$$

Boundary conditions are equals to $T(0) = T(L) = T(0)$. Paying attention to the equation (6) and the conditions mentioned, the temperature function can be as following:

$$T(x) = \frac{v^2}{2\rho KL^2}(L-x)x + T_0 \tag{7}$$

By imposing the thermal gradient perpendicular to the model axis, the thermal transfers are:

$$T(x) = (T-T_0)x/L + T_0 \tag{8}$$

$$T(y) = \frac{T_{hot}-T_{cold}}{h}y + \frac{T_{hot}-T_{cold}}{2}, \tag{9}$$

where T_{cold} and T_{hot} are the cold and hot temperatures, respectively. Deformation in

coordinates $X-Y$ can be shown by the parameter of $v(x)$. Assume waiving the $Y-Z$ planes deformation, the theoretical calculations can be as following:

$$\frac{\partial^2}{\partial x^2}\left(EI\frac{\partial^2 v}{\partial x^2}\right) = F - P\frac{\partial^2 v}{\partial x^2}, \quad (10)$$

where I, P and f is moment of inertia, Young's modulus, load of the model and force, respectively, hence:

$$F = P(x) - \frac{\partial^2 \int \alpha E T y dA}{\partial x^2} \quad (11)$$

Thermal expansion coefficient is α. By solving equation (11) following equation can be found:

$$\int \alpha E T y dA = \frac{\alpha E w h^2}{12}(T_{hot} - T_{cold}) \quad (12)$$

Because of waiving the movement in $Y-Z$:

$$\int \alpha E T z dz = M_{Ty} \quad (13)$$

So:

$$\frac{\partial^2 \int \alpha E T y dA}{\partial x^2} = 0 \quad (14)$$

Substituting Equation (13) into (10), shows $F = 0$, hence:

$$\frac{\partial^4 v}{\partial x^4} EI + P\frac{\partial^2 v}{\partial x^2} = 0 \quad (15)$$

Assuming the right end is free or unsupported, $P = 0, \frac{\partial v(0)}{\partial x} = v(0) = 0$. By considering the thermal stresses, the boundary conditions at the free end of a solid beam are:

$$EI\frac{\partial^2 v}{\partial x^2}(L) = -\int \alpha E T y dA, \quad (16)$$

$$EI\frac{\partial^3 v}{\partial x^3}(L) = -P\frac{\partial V}{\partial x} - \frac{\partial \int \alpha E T y dA}{\partial x} \quad (17)$$

According to equation (12):

$$12I\frac{\partial^2 v}{\partial x^2}(x) = -\alpha w h^2 (T_{hot} - T_{cold}) \quad (18)$$

Using the boundary conditions and integrating the equation (18), deformation equation is:

$$v(x) = \frac{-\alpha w h^2 (T_{hot} - T_{cold}) x^2}{24 \int y^2 dA}, \quad (19)$$

and

$$\int y^2 \, dA = \frac{w h^2}{12} = I \quad (20)$$

Finally, Equation (19) converts to (21):

$$v(x) = \frac{-\alpha (T_{hot} - T_{cold}) x^2}{24h} \quad (21)$$

By substituting equation (7) in equation (21), the deformation value of the slider can be calculated. To calculate deformation of the slider, there is another solution. Variable T is the temperature of the constrainer block, and the temperature variable of the hot arm is $+\Delta T$. Variable T causes deformation in the structure. In other words, the temperature difference cause arm to be elongated. Dimensions of the constrainer especially remain no change and cause the slider to an up-ward deformation. The vertical deformation $disp_\alpha$, the arms dimensions $disp_T$ and the temperature difference ($disp_{\Delta T}$) can be approximated by [5, 19]:

$$disp_\alpha = disp_T + disp_{\Delta T \approx} \alpha C(T \sin\beta + \frac{\Delta T}{\sin\beta \cos\beta}) \cong \alpha C(T\beta + \Delta T \beta^{-1}) \quad (22)$$

Assuming similarity of T and ΔT of 2 cells:

$$disp_\alpha \cong 2 disp_T = \alpha(TA + 2C\Delta T\beta^{-1}) \quad (23)$$

ΔT and $N_{\Delta T}$ approximately can be found:

$$N_{\Delta T} \cong \frac{\alpha \Delta T}{(\sin\beta)^2} + \frac{12Ep(\cos\beta)^2}{0.25C^2} \quad (24)$$

where p is moment of inertia; this force lonely may cause the arm to be buckled. The axial compressive force in the arm can approximately be found by [5]:

$$N \cong \frac{\alpha \Delta T}{(\sin\beta)^2} + \frac{12Ep(\cos\beta)^2}{0.25C^2} + \frac{F}{2\sin\beta} \quad (25)$$

The *LMA* proposed is made of polysilicon. The dimension of the whole *LMA*'s structure clearly has given in Table 1.

Table 1. Dimensions of the slider and the comb drive.

Parameter	Value (μm)	Parameter	Value (μm)
M	35	Z	55
A	1600	G	10
B	350	U	24
C	800	O	14
D	50	R	3
E	100	S	2
F	1000	Y	3

Table 2 shows the material properties of polysilicon. Dimensions are in the micrometer scale and the parameters have been normalized due to *ANSYS* software technical conditions. The slider experiences a stroke of 2.1 μm, as shown in Fig. 6, by applying a DC voltage 13 volt. A minimum step size

of 1 μm can be achieved, by applying a DC voltage of 7 volt to electrode of the slider. Figs. 7 and 8 illustrates the slider Expansion normally versus to the voltage applied and the time, respectively. Fig. 9, also shows the slider force generated versus the voltage applied. The maximum temperature distribution over the structure is 450 ℃.

Table 2. The Polysilicon properties used in the simulation.

Para	Value	Unit
Dens	2.33	$pg.\mu m^{-2}$
Ex	169	$pg.\mu m^{-1}ns^{-2}$
Prxy	0.28	-
Th ex	$2.6e^{-6}$	$℃^{-1}$
Res	e^{9}	$\mu m.\Omega$
Thermal conductivity	$14.9e^{-5}$	$pg.\mu m.ns^{-3}℃^{-1}$

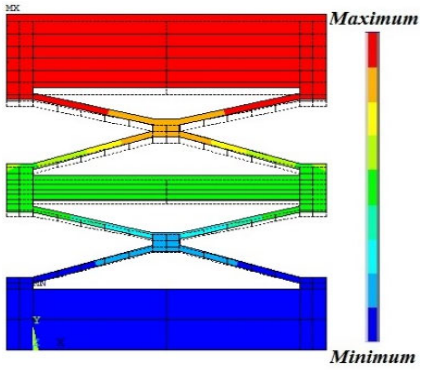

Fig. 6. Contour plots of the slider deformation.

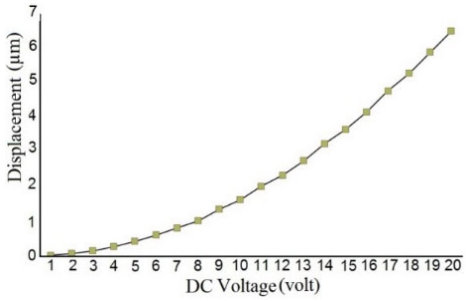

Fig. 7. Expansion of the slider vs. the DC voltage applied.

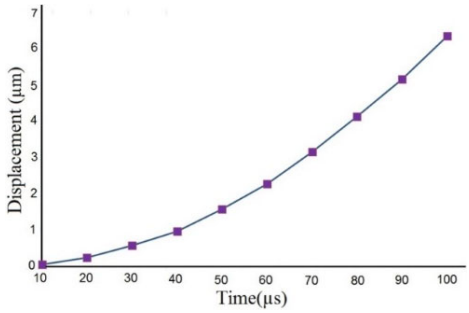

Fig. 8. Expansion of the slider vs. the time.

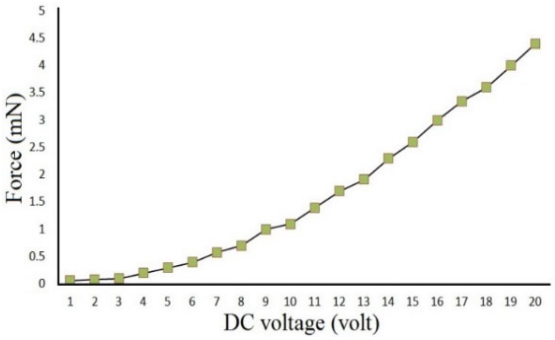

Fig. 9. The force generated of the slider vs. the DC voltage applied.

2.3. Designing of the Stopper

One of the main parts of the actuator proposed, shown in Fig. 10, is the stopper. It mainly consists of three parts; the clutch, the electrostatic comb drives and anchors. The friction generated by clutches, causes the slider stop moving. Some the linear actuators use the clutch and the notch. These types of the actuators generate powerful static force. At beginning of the design, the maximum amount of the force generated by the slider should be considered. Take into consideration which the static friction force generated by the clutches must overcome the slider propulsion force generated. There are two ideas to design the springy clutch. The low springy stiffness of the clutch results a required low electrostatic force; and vice versa. With the high springy stiffness, the clutches require more the actuation voltage to be activated, so there is a trade-off between the springy stiffness presented in the equation (26) and the static friction force; where N is elastic potential of the clutch. Because of using the notches [20], the friction force generated is appropriately large. The comb drives are used to trigger the clutch to prevent the slider from any shaking or movement. The comb drive can ideally be modeled as a set of *m* conductors. These conductors are embedded in a uniform lossless dielectric medium (see Fig. 11). Conductors have constant electrostatic potential ability. The charges are equally distributed on conductor's surface [14].

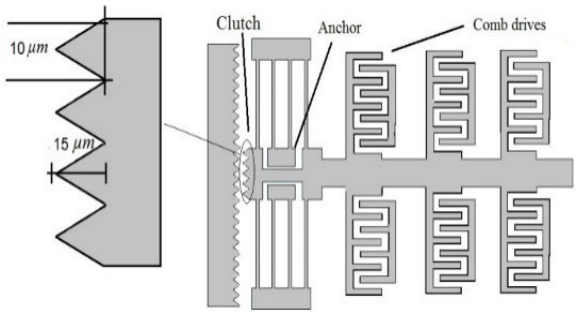

Fig. 10. Schematic of the stopper.

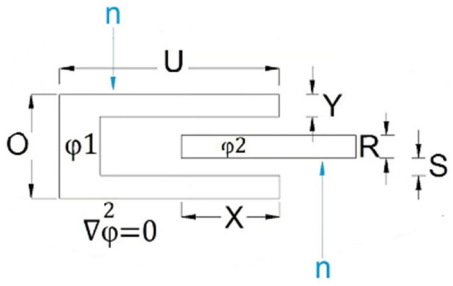

Fig. 11. Schematic view of a comb drive cell.

$$F = \mu_S N, \tag{26}$$

$$q_{i(v)} = \varepsilon \frac{\partial \varphi_i(v)}{\partial n}, \tag{27}$$

where $q_{i(v)}, \varepsilon, \varphi_i, i$ *and* n are the charge density on the surface, the dielectric constant, the conductor electrostatic potential, the internal region and the external region of the conductors, respectively:

$$\nabla^2 \emptyset = 0 \tag{28}$$

Here i is the number of conductors. By considering the boundary conditions $\varphi = \varphi_i$ and having $i = 1, 2, 3, m$, the surface charge density can be obtained:

$$\emptyset_i = \sum_{j=1}^{m} {}_{\partial sl} \int \frac{\partial \varphi}{\partial n}(v')\, G(v, v') d_{surf}(v') + \hat{K}, \tag{29}$$

$$Q = \sum_{j=1}^{m} {}_{\partial sl} \int \frac{\partial \varphi}{\partial n}(v')\, d_{surf}(v') \tag{30}$$

where Q, G, v and v′ are the total charge, the Green's function, the position vector of source point and position vector of field point, respectively. ∂S_l is the surface of conductor J, which is zero and K is a constant. Electrostatic force is equal to:

$$f = -\frac{1}{2}\frac{q^2}{\varepsilon} n, \tag{31}$$

$$F = \int f_x ds_\Gamma, \tag{32}$$

where f_x is the component x of the force, Γ is the surface of the moving finger [14]. Therefore, the comb drive dimensions can be established; dimensions are presented in Table 1. Fig. 12(a) and 12(b), respectively, shows the model meshed of the springy clutch and its deformation by applying a force equal to 50 μN. Fig. 13 depicts deformation of the clutch versus the force applied by the comb drives. Fig. 14 shows the force generated by single cell of the comb drive. A force more than 50 μN can be generated by applying a voltage 10 volt to the comb drives which is enough to push the clutches toward the substrate side walls. It should be noted that the electrostatic actuation block must be isolated from the slider´s body. This isolation is necessary to prevent errors due to interaction of the electro-thermal and electrostatic circuits. The material selected to be used as an isolator can be SIO_2. Figs. 15 and 16 show stress contours of the springy clutch during process; there is a maximum stress of 0.56 GPA and 0.6 GPA, respectively, which is logically acceptable.

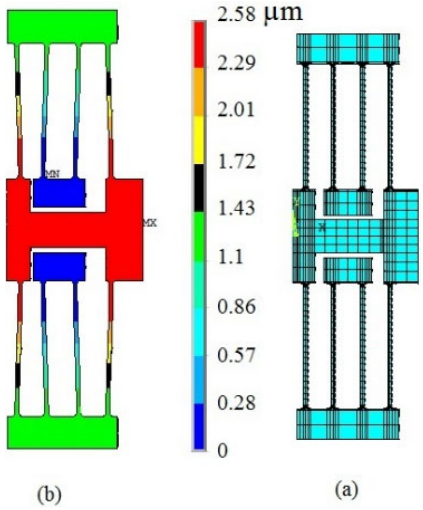

Fig. 12. A model deformed of the springy clutch (a), contour plots of the clutch deformation by applying a force equal to 50 μN and a deformation equal to 2.58 μm.

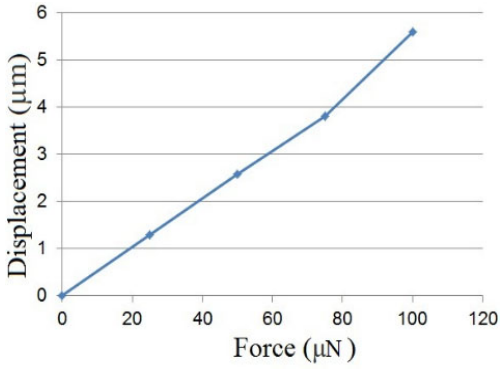

Fig. 13. Deformation of the clutch vs. the force generated of the comb drives.

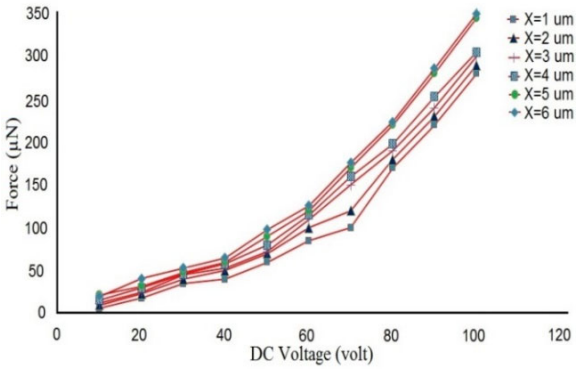

Fig. 14. The force generated of a comb drive vs. the DC voltage applied.

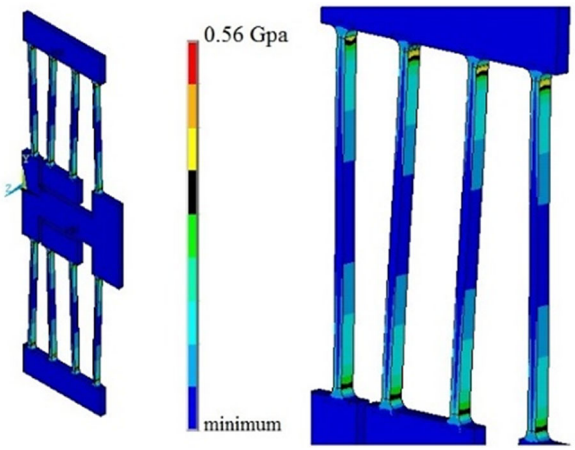

Fig. 15. Stress contour plots of the springy clutch by applying a force equal to 2 mN (+y direction).

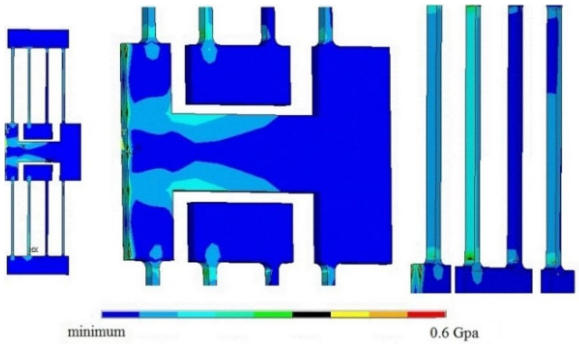

Fig. 16. Stress contour plots of the springy clutch while applying a force equal to 2.2 mN (+y direction).

3. Conclusion

The *LMA* proposed can achieve stroke of 2.1 μm with the acceptable force generated of 2 mN. By repeating the operational sequences numerous times, large travel range can be achieved. The actuator presented has minimum step size about 2.1 μm so that makes this opportunity for CCD Camera´s Lens to have a high resolutions and accuracy. To increase the friction force, there are many techniques, but in this work, two ideas were followed; first, increasing the numbers of the comb drives which results increasing whole the system size. Secondly, using impact stator head and the sliders with the edges notched. These two ideas have pros and cons so it should be taken into consideration technologically. The simulation results show that the *LMA* proposed has good speed, high accuracy and large travel range precisely to be used in adjusting CCD Camera´s Lens.

References

[1]. M. Baltzer, T. Kraus, T. Obermeier, A linear stepping actuator in surface micromachining technology for low voltages and large deflections, in *Proceedings of the IEEE Conference Solid-State Sensors and Actuators*, Chicago, IL, 1997, pp. 781-784.

[2]. K. Chinzei, R. Kikinis, F. Jolesz, Compatibility of mechatronic devices: designs criteria, in *Proceedings of the Medical Image Computing and Computer-Assisted Intervention*, 1999, pp. 1020-1030.

[3]. M. J. Daneman, N. C. Tien, O. Solgaard, A. P. Pisano, K. Y. Lau, R. S. Muller, Linear microvibromotor for positioning optical components, *J. Microelectromech. Syst.*, Vol. 5, 1996, pp. 159-165.

[4]. Q. A. Huang, N. K. S Lee, Analytical modeling and optimization for a laterally driven polysilicon thermal actuator, *Microsystem Technologies*, Vol. 5, Issue 3, 1999, pp. 133-137.

[5]. D. Hill, W. Szyszkowski, E. Bordatchev, On modeling and computer simulation of an electro-thermally driven cascaded nickel microactuator, *Sensors and Actuators A*, Vol. 126, 2006, pp. 253-263.

[6]. Y. Kuang, Q. A. Huang, N. K. S. Lee, Numerical simulation of a polysilicon thermal flexure actuator, *Microsystem Technologies*, Vol. 8, 2002, pp. 17-21.

[7]. H. N. Kwon, S. H. Jeong, S. K. Lee, J. H. Lee, Design and characterization of a micromachined inchworm motor with thermoelastic linkage actuators, *Sensors Actuators A*, Vol. 103, 2003, pp. 143-149.

[8]. C. S. Pan, W. Hsu, An electro-thermally and laterally driven polysilicon microactuator, *J. Micromech. Microeng*., Vol. 7, 1997, pp. 7-13.

[9]. M. Pai, N. C. Tien, Low voltage electrothermal vibromotor for silicon optical bench applications *Sensors Actuators A*, Vol. 83, 2000, pp. 237-243.

[10]. J. S. Park, L. L. Chu, A. D. Oliver, Y. B. Gianchandani, Bent-beam electrothermal actuators: II. Linear and rotary microengines, *J. Microelectromech. Syst*., Vol. 10, 2001, pp. 255-262.

[11]. J. R. Reid, V. M. Bright, J. T. Butler, Automated assembly of flip-up micromirrors, *Sensors Actuators A*, Vol. 66, 1998, pp. 292-298.

[12]. T. Risaku, Y. Eui-Hyeok, A normally latched large-stroke, inchworm microactuator, *Micromech. Microeng*., Vol. 17, 2007, pp. 1715-1720.

[13]. N. R. Tas, T. Sonnenberg, R. Molenaar, M. Elwenspoek, Design, fabrication and testing of laterally driven electrostatic motors employing walking motion and mechanical leverage, *J. Micromech. Microeng.*, Vol. 13, 2003, pp. N6-N15.

[14]. Y. Wenjing, M. Subrata, C. M. Noel, Optimal shape design of an electrostatic comb drive in microelectro-mechanical systems, *Journal of Microelectromechanical Systems*, Vol. 7, Issue 1, 1998, pp. 16-26.

[15]. H. Yamashita, H. Nozue, E. Nomura, K. Itoh, T. Ema, S. Hirasawa, K. Kojima, T. Tamura, K. Nakajima, Recent progress in electron-beam cell projection technology, *Jpn. J. Appl. Phys. 1: Regul. Pap*., Vol. 35, Issue 12B, 1996, pp. 6404-6414.

[16]. R. Yeh, S. Hollar, K. S. J. Pister, Single mask, large force, and large displacement electrostatic linear inchworm motors, *J. Microelectromech. Syst*., Vol. 11, 2002, pp. 330-336.

[17]. C. Shao, S. Liu, Y. Hao, K. Ma, Research on electrothermal actuator applied in MEMS safety system, in *Proceedings of the 2nd International Conference on Machine Learning and Computer Application (ICMLCA'21)*, Shenyang, China, 17-19 December 2021, pp. 1-8.

[18]. R. Saba, S. Iqbal, R. I. Shakoor, M. M. Saleem, S. A. Bazaz, Design and analysis of four-jaws

microgripper with integrated thermal actuator and force sensor for biomedical applications, *Rev. Sci. Instrum*., Vol. 92, 2021, 045007.
[19]. A. S. Algamili, M. H. Md. Khir, J. O. Dennis, A. Y. Ahmed, S. S. Alabsi, S. S. Ba Hashwan, M. M. Junaid, A review of actuation and sensing mechanisms in MEMS-based sensor devices, *Nanoscale Research Letters*, Vol. 16, 2021, 16.
[20]. S. Evstafyev, V. Samoylikov, S. Timoshenkov, P. Gornostaev, Designing thermal MEMS on a system level, *Proceedings of SPIE*, Vol. 12157, 2022, 121570M.
[21]. N. M. Kommanaboinaa, M. F. Pantano, A. Bagolini, Optimization of an amplification mechanism enabling large displacements in MEMS-based nanomaterial testing devices, *Micro and Nano Engineering*, Vol. 15, June 2022, 100131.